Geophysical Research Letters

RESEARCH LETTER
10.1029/2021GL093337

Gravitational Circulation as Driver of Upstream Migration of Estuarine Sand Dunes

W. M. van der Sande[1], P. C. Roos[1], T. Gerkema[2], and S. J. M. H. Hulscher[1]

[1]Department of Water Engineering and Management, University of Twente, Enschede, The Netherlands, [2]Department of Estuarine and Delta Systems, NIOZ Royal Netherlands Institute for Sea Research, Yerseke, The Netherlands

Key Points:

- Model results show that gravitational circulation, if sufficiently strong compared to river flow, causes upstream dune migration
- Unlike in marine sand wave models, migration direction does not necessarily coincide with the tide-averaged sediment transport direction
- This is the first time that gravitational circulation has been included in a process-based model of sand wave/dune formation

Correspondence to:
W. M. van der Sande,
w.m.vandersande@utwente.nl

Citation:
van der Sande, W. M., Roos, P. C., Gerkema, T., & Hulscher, S. J. M. H. (2021). Gravitational circulation as driver of upstream migration of estuarine sand dunes. *Geophysical Research Letters*, *48*, e2021GL093337. https://doi.org/10.1029/2021GL093337

Received 19 APR 2021
Accepted 9 JUN 2021

Abstract Sand dunes are large-scale rhythmic bed patterns commonly occurring in sandy shelf seas, estuaries and rivers. Field observations of sand dunes in the Gironde estuary (France) have suggested that the gravitational circulation may cause seasonal reversal of asymmetry, which is linked to migration direction. In this study, we aim to unravel the influence of gravitational circulation on the migration of estuarine sand dunes. To this end, we present an idealized process-based sand dune model with tide and river forcing, and the addition of a longitudinal salinity gradient (imposed diagnostically) that induces gravitational circulation. Linear stability analysis shows the emergence of dunes from a flat bed and confirms that reversal of dune migration may occur, provided the gravitational circulation is sufficiently strong compared to the river flow velocity. Lastly, we show that the migration direction of estuarine sand dunes is not necessarily the same as the direction of net sediment transport.

Plain Language Summary Many sea and river beds are covered with large-scale rhythmic patterns, termed sand dunes. These are dynamic patterns in the bed that grow and move (i.e., migrate). They also occur in the transition zone between seas and rivers: estuaries. Estuarine sand dunes are not only subject to a mixture of riverine and marine processes, but also influenced by several estuarine-specific processes. Here, we focus on the gravitational circulation, which stems from the interaction between heavier salt water and lighter freshwater. In this research, we develop a simulation model which reveals how this affects the migration of estuarine sand dunes. Our model results explain how gravitational circulation, if strong enough compared to the river flow, can cause upstream migration of these bedforms, that is, against the river flow.

1. Introduction

Estuaries are water bodies in which a river meets a sea or ocean. In many of those, sand dunes can be found. These are large-scale rhythmic bed patterns with their crest oriented roughly perpendicular to the flow, and they have heights and wavelengths in the order of meters and hundreds of meters, respectively (Allen, 1976; Berné et al., 1993; Kostaschuk & Best, 2005). Their dimensions and dynamic nature pose a threat to local infrastructure, and they possibly govern the flow roughness (Best, 2005), just like their marine (Damveld et al., 2018) and riverine counterparts (Gensen et al., 2020).

One particular process that is of interest (and which is the subject of this study) is the gravitational circulation, characteristic of estuaries. That is, the salinity difference between river and sea or ocean results in a longitudinal salinity and density gradient in the estuary. This density gradient entails a baroclinic pressure gradient, which in turn induces a circulation characterized by a tidally averaged residual current that is directed downstream (seaward) at the surface, and upstream (landward) near the bed. The intensity of the gravitational circulation is proportional to the longitudinal salinity gradient, and it constitutes one component of the estuarine circulation (Geyer & MacCready, 2014).

Since near-bed flow is responsible for most of the sediment transport, it is plausible that gravitational circulation influences the dimensions and dynamics of estuarine sand dunes. Berné et al. (1993) used this reasoning to explain observations of dune dynamics in the Gironde estuary, France. There, dunes occur in the lower estuary where they have wavelengths of around 100 m. Between their two measurement campaigns, these dunes had swapped asymmetry from landward to seaward (which is commonly related to migration direction; Knaapen, 2005), possibly due to the salinity-induced gravitational circulation.

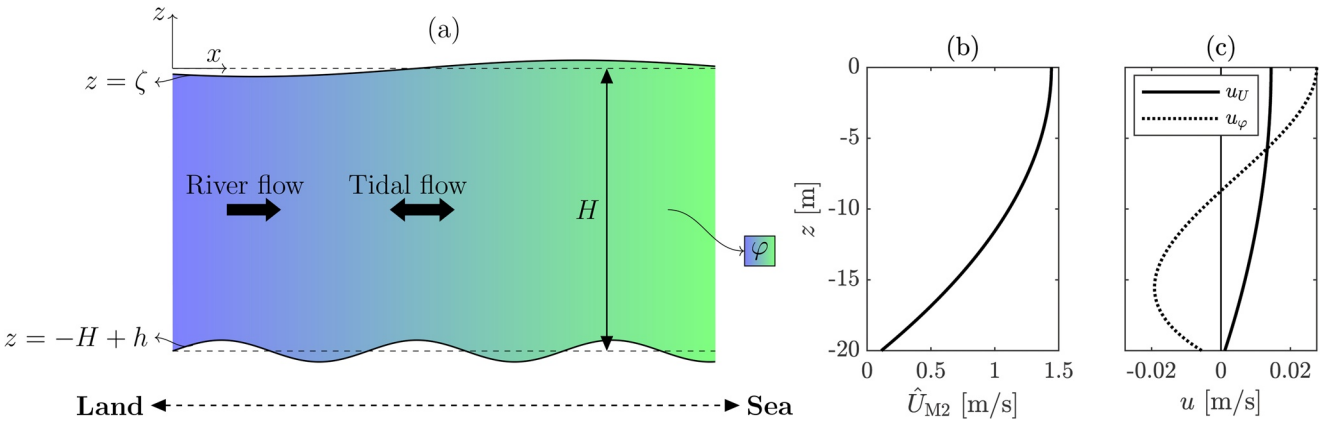

Figure 1. (a) Overview of the model domain, showing a local portion of an estuary with mean depth H, free surface elevation ζ and bed topography h. It is subject to river flow, tidal flow and estuarine circulation driven by the longitudinal salinity gradient φ. (b, c) Solution to the basic state as derived in Section 3.2, consisting of (b) the tidal flow amplitude $\hat{U}_{M2}(z)$ and (c) the river flow u_U with depth-averaged velocity U_{res}, and the gravitational circulation u_φ with zero depth-averaged flow velocity; parameter values given in Table 1.

In this study, we aim to unravel the effect of the longitudinal salinity gradient on estuarine sand dunes through an idealized process-based model which includes gravitational circulation through the classical approach (Hansen & Rattray, 1965), and which further contains essential processes such as tidal flow, river flow and sediment transport. With this model, we perform a linear stability analysis, which yields the preferred bedform length of the system and its corresponding growth and migration rate. Such models have been used in past research to explain river dunes (Engelund, 1970; Paarlberg et al., 2009) and marine sand waves (Campmans et al., 2017; Hulscher, 1996) as free instabilities of the system. This study is the first to use this method to shed light upon the driving mechanisms behind these bedforms in the estuarine setting.

This study proceeds with the model description (Section 2), whereupon it presents the solution procedure (Section 3), of which the implementation is made publicly available (van der Sande et al., 2021). After that, model results are shown (Section 4), and the discussion section will further elaborate on the application of this model to the Gironde (Section 5) before the final conclusions are drawn (Section 6).

2. Model Formulation

2.1. Geometry and General Assumptions

We present an idealized process-based model which represents a local portion of a well-mixed estuary (Figure 1), with the parameter values inspired by the Gironde setting (Table 1). These originate from the following observations of Berné et al. (1993): large tidal current amplitude, whereas wind-driven currents are small and wave action is insignificant; sand is medium to coarse. We consider a single tidal constituent (i.e., a symmetric tide), and—with regard to migration—we thereby focus our modeling approach on isolating the effect of gravitational circulation from that of tidal asymmetry (which is another potential driver of migration; Besio et al., 2004).

The local character of our model implies that we need to impose variables which stem from interactions on a larger scale. In our diagnostic modeling approach, we thus impose the longitudinal salinity gradient as well as tidal and river flow, and as such do not model the inherent coupling of these three variables. Instead, in the application to the Gironde estuary, we use data from the numerical model of van Maanen and Sottolichio (2018) which covers the entire Gironde estuary.

The model covers a 2DV domain with the horizontal x-coordinate in longitudinal direction (positive is seaward and negative is landward) and the vertical z-coordinate directed upward; u and w denote the horizontal and vertical velocity, respectively. Furthermore, ζ is the vertical displacement of the water surface with respect to the mean (which is defined at $z = 0$). The bed profile is located at $z = -H + h$, with H the mean depth and h describing the bed topography. The horizontal boundary conditions are spatially periodic.

Table 1
Model Parameters With the (Range in) Values Reflecting the Gironde Setting, for Both a Low and High Discharge Scenario

Symbol	Description	Value		Units
U_{M2}	Depth-avg. M2 velocity amplitude[a]	1		$m\ s^{-1}$
β	Contraction coefficient	7.6×10^{-4}		psu^{-1}
H	Mean water depth[a]	20		m
c_d	Drag coefficient	2.5×10^{-3}		–
A_v	Vertical eddy viscosity	0.05		$m^2\ s^{-1}$
s	Slip parameter[d]	0.04		$m\ s^{-1}$
ω	M2 tidal frequency	1.405×10^{-4}		s^{-1}
α_b	Bed load coefficient[e]	1.56×10^{-5}		$m^{7/2}\ s^2\ kg^{-3/2}$
β_b	Bed load exponent[e]	1.5		–
λ	Slope correction factor[f]	1.5		–
ρ	Water density	1020		$kg\ m^{-3}$
p	Bed porosity	0.4		–
		Low discharge	High discharge	
φ	Longitudinal salinity gradient[b]	0–0.3	0.9–1.3	10^{-3} psu m^{-1}
Q_{res}	River discharge[a,b]	250–400	1000–1750	$m^3\ s^{-1}$
U_{res}	Depth-avg. river flow velocity[c]	0.31–0.5	1.3–2.2	$cm\ s^{-1}$

[a]Berné et al. (1993). [b]van Maanen and Sottolichio (2018). [c]Following from $U_{res} = Q_{res}/A$, with $A = 8 \times 10^4\ m^2$, see Section 5.1 for substantiation. [d]Calibrated. [e]Meyer-Peter and Müller (1948). [f]Bagnold (1956).

In this study, model equations are shown in their dimensional form. A scaling procedure as performed by for example Campmans et al. (2017) (not shown here) reveals that boundary conditions may be applied at $z = 0$ instead of $z = \zeta$, which is also known as the rigid-lid approximation. Furthermore, we assume homogeneity in the second horizontal direction, and we neglect the Coriolis force since its effect on sand dunes is typically minor (Hulscher, 1996) and because our local model is, by definition, not capable of capturing the Coriolis effects at the estuarine scale. Also, we apply the Boussinesq approximation, which states that variations in density are considered negligible except those involved in the gravity term.

Following earlier marine sand wave studies, we use the simplest turbulence closure model with a constant eddy viscosity and a partial slip condition at the bed (van Haren & Maas, 1987). This means that we do not account for variations of the eddy viscosity with flow intensity (e.g., Borsje et al., 2013) and stratification (e.g., Geyer & MacCready, 2014), the latter being known to further strengthen the estuarine circulation. Also, we only consider bed load transport of non-cohesive sediment with uniform grain size, without a critical shear stress. We disregard suspended sediment transport, because the sediment grain size at the Gironde estuary sand wave field is relatively large, and because bed load already captures the main mechanism behind sand wave formation (Hulscher, 1996).

2.2. Water Motion

Water motion is modeled through the hydrostatic shallow water equations (not depth-averaged):

$$\frac{\partial u}{\partial t} + u\frac{\partial u}{\partial x} + w\frac{\partial u}{\partial z} = A_v\frac{\partial^2 u}{\partial z^2} - g\frac{\partial \zeta}{\partial x}\underbrace{-F_{btr}^{steady} - F_{btr}^{osc} - F_{bcl}}_{\text{Forcing terms}}, \tag{1a}$$

$$\frac{\partial u}{\partial x} + \frac{\partial w}{\partial z} = 0, \tag{1b}$$

in which g is the gravitational acceleration, and A_v is the (spatially uniform) vertical eddy viscosity approximated by $A_v = c_d H U_{M2}$, with drag coefficient $c_d = 2.5 \times 10^{-3}$ (Prandle, 1985), and U_{M2} the depth-averaged tidal velocity amplitude. To reflect the estuarine setting, we consider three forcing terms:

$$\begin{aligned} F_{\text{btr}}^{\text{steady}} &= B_{\text{res}} && \textbf{steady } \textbf{baro}\textbf{tr}\text{opic forcing;} \\ F_{\text{btr}}^{\text{osc}} &= B_{M2}\exp(i\omega t) + \text{c.c.} && \textbf{osc}\text{illatory } \textbf{baro}\textbf{tr}\text{opic forcing;} \\ F_{\text{bcl}} &= -g\beta\varphi z && \text{salinity-induced } \textbf{baro}\textbf{cl}\text{inic forcing.} \end{aligned} \tag{2}$$

Here, β is the contraction coefficient (in psu^{-1}), φ the longitudinal salinity gradient (in psu m^{-1}) and B_{res} is the river-induced forcing. Furthermore, we include the M2-tide with forcing amplitude B_{M2}.

These equations are supplemented with two boundary conditions at both the surface and the bed. At the surface, we impose zero shear stress (ignoring local wind forcing) and a kinematic boundary condition which demands particles at the surface to "follow" the water surface. Because $\text{Fr}^2 = U_{M2}^2/(gH) \ll 1$, the latter condition results in a vanishing vertical water velocity. The rigid lid approximation allows us to apply the boundary conditions at $z = 0$:

$$\frac{\partial u}{\partial z} = 0, \quad w = 0 \qquad \text{at } z = 0. \tag{3}$$

In a similar fashion, there are two boundary conditions at the bed, which are the partial slip condition and a kinematic condition demanding water particles at the bed to follow the bed profile. These conditions, applied at $z = -H + h$, are given by

$$\frac{\tau_b}{\rho} \equiv A_v \frac{\partial u}{\partial z} = su, \quad w = u\frac{\partial h}{\partial x} \qquad \text{at } z = -H + h, \tag{4}$$

with τ_b the bed shear stress, s the slip parameter and ρ the water density which is kept constant in accordance with the Boussinesq assumption.

2.3. Sediment Transport and Bed Evolution

Bed load transport is modeled as a power of the local bed shear stress with a gravitational correction (Bagnold, 1956):

$$q_b = \alpha_b |\tau_b|^{\beta_b} \left(\frac{\tau_b}{|\tau_b|} - \lambda \frac{\partial h}{\partial x} \right), \tag{5}$$

with bed load coefficient α_b, exponent $\beta_b = 1.5$ and bed slope parameter λ. Finally, bed evolution is given by the Exner equation:

$$(1 - p)\frac{\partial h}{\partial t} = -\frac{\partial \langle q_b \rangle}{\partial x}, \tag{6}$$

where p is the bed porosity, and $\langle \cdot \rangle$ denotes tidal averaging. By taking the tidal average, we use that the morphodynamic timescale is much larger than the tidal timescale.

3. Solution Procedure

3.1. Expansion

We analyze the behavior of the system as defined in Section 2 through a linear stability analysis of a basic state characterized by a spatially uniform flow and sediment transport over a horizontally flat bed. This basic state is then perturbed through small-amplitude perturbations in the bed topography:

$$h = h_0 + h_1, \qquad h_0 = 0, \qquad h_1 = \hat{h}_1 \exp(\mathrm{i}kx) + \text{c.c.} \tag{7}$$

Here, k is the (real-valued) topographic wavenumber and $\hat{h}_1$ the (complex) amplitude which may evolve over time. Truncating at first order is valid for $\left|\hat{h}_1\right| \ll H$, which encompasses the stage of initial growth. Analogous to Equation 7, the other unknowns are also expanded as a superposition of a basic and perturbed state:

$$\begin{aligned} u &= u_0 + u_1, \qquad w = w_0 + w_1, \qquad \zeta = \zeta_0 + \zeta_1, \\ \tau_b &= \tau_{b,0} + \tau_{b,1}, \quad q_b = q_{b,0} + q_{b,1}. \end{aligned} \tag{8}$$

Finally, we solve for the perturbed bed amplitude $\hat{h}_1(t;k)$, that is, the bedform's amplitude function of time for some topographic wavenumber k.

3.2. Basic State

Analytical expressions of the basic flow and sediment transport are found through integrating the model equations and applying the boundary conditions. First, we may directly conclude that $w_0 = 0$, because $\partial u_0/\partial x = 0 = -\partial w_0/\partial z$ (horizontal invariance of the solution) and the vertical velocity at both boundaries is zero. Furthermore, the horizontal invariance implies that $\partial\zeta_0/\partial x = 0$, and thus $\zeta_0 = 0$.

The solution to the horizontal water motion can be composed of a superposition of the solutions to the three different forcing mechanisms: $u_0 = u_{0,\mathrm{bcl}} + u_{0,\mathrm{btr}}^{\mathrm{steady}} + u_{0,\mathrm{btr}}^{\mathrm{osc}}$. Analytical expressions of these three terms are given in Appendix A. Choosing B_{res} such that the depth-averaged and tidally averaged velocity equals U_{res} yields two terms (Figure 1b and 1c): One with zero depth-averaged flow representing the gravitational circulation (u_φ), and another with its depth-averaged flow equal to U_{res} which represents the river flow (u_U). This is usually done in modeling of the gravitational circulation (Hansen & Rattray, 1965; Geyer & MacCready, 2014).

Although the sediment transport in the basic state is nonzero, there is no divergence of it, and thus there is also no bed evolution.

3.3. Perturbed State

The perturbed flow and sediment transport are found through integration of the model equations. The Exner Equation 6 is then used to arrive at the growth equation for the bed amplitude $\hat{h}_1$:

$$\frac{\mathrm{d}\hat{h}_1}{\mathrm{d}t} = \gamma\hat{h}_1 \quad \Rightarrow \quad \hat{h}_1(t) = \hat{h}_{\mathrm{init}} \exp(\gamma t). \tag{9}$$

This exponential growth is characterized by a complex growth rate $\gamma = \gamma_r + \mathrm{i}\gamma_i$, with γ_r the growth rate and $-\gamma_i/k = c_{\mathrm{mig}}$ the migration rate. An example of a growth curve and corresponding migration curve that describe the function $\hat{h}_1(t;k)$ is given in Figures 2a and 2b.

Physically, the results must be interpreted as follows: If there exists at least one wavenumber which results in a positive growth rate γ_r, the flat bed is unstable and bedforms will develop. The wavenumber with the largest growth rate (termed the fastest growing mode [FGM]) is assumed to be the mode that is preferred by the system. Van Santen et al. (2011) showed that the FGM indeed shows good agreement with field observations when the value of the slip parameter s is chosen appropriately. Here, we adopt the same approach and thus choose the value of s such that the FGM matches the wavelengths found by Berné et al. (1993) in the Gironde estuary (≈100 m).

4. Results

Table 1 shows the (range in) parameter values which are used in our model runs. Results for a fixed river flow and varying longitudinal salinity gradient are given in Figures 2c–2e, which shows that the growth rate and the wavelength of the FGM are almost insensitive to variations in the longitudinal salinity gradient

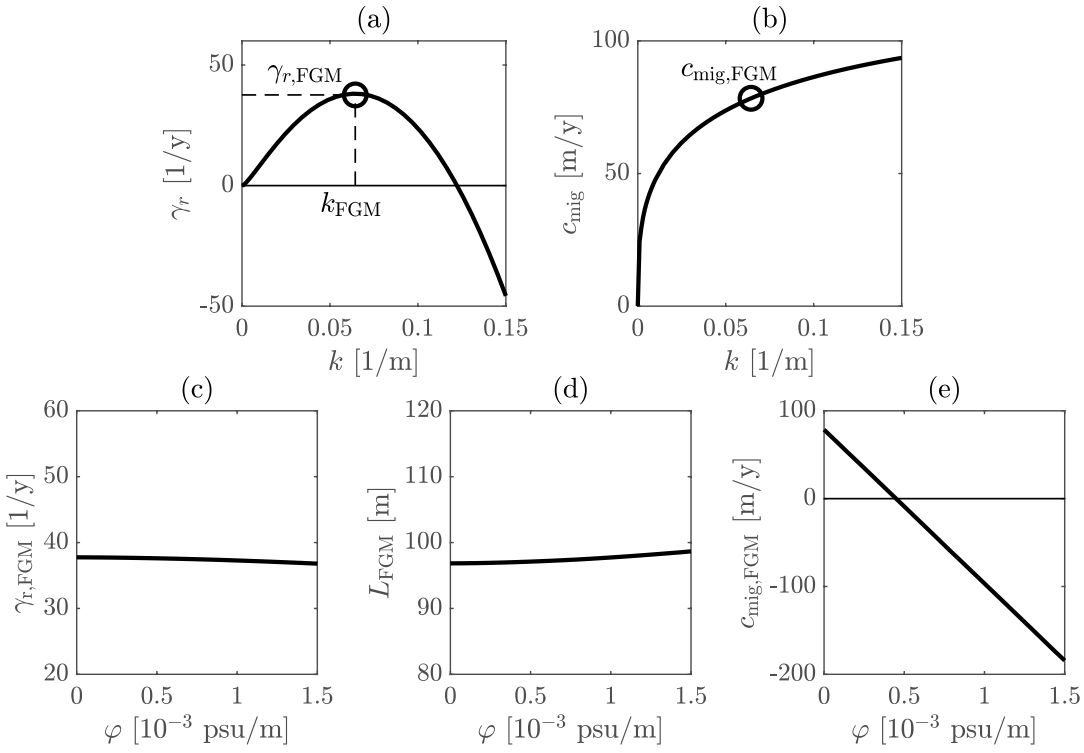

Figure 2. (a) Example of a growth curve and (b) Corresponding migration rate for $\varphi = 0$ and $U_{\mathrm{res}} = 0.01$. The fastest growing mode (FGM) is denoted with the circle, with $L_{\mathrm{FGM}} = 2\pi/k_{\mathrm{FGM}} = 98$ m and $c_{\mathrm{mig,FGM}} = 78$ m y^{-1}. Sensitivity of the fastest growing mode properties to the salinity gradient (again with $U_{\mathrm{res}} = 0.01$ m s^{-1}): (c) growth rate, (d) wavelength, both showing little variation, and (e) migration rate, which shows large variations. Parameter values as given in Table 1.

(Figures 2c and 2d, respectively). Hence, we limit the further analysis to salinity effects on the migration rate.

From Figure 2e, it becomes clear that the migration rate may reverse depending on the strength of the longitudinal salinity gradient. This already demonstrates that the gravitational circulation may give rise to upstream migration of estuarine sand dunes.

The combined sensitivity of the migration rate to the depth-averaged river flow velocity and the longitudinal salinity gradient for both the default parameter settings and to a variety of changed parameter settings is shown in Figure 3. All plots in Figure 3 share the same qualitative message: Gravitational circulation may cause upstream (negative) migration rates, provided the river flow velocity is small compared to the gravitational circulation. The leftmost tile of Figure 3 also marks two cases for the Gironde estuary: one during low discharge and one during high discharge conditions. These correspond to the two cases studied by Berné et al. (1993), and will be further elaborated on in the discussion (Section 5.1).

Figure 3 also shows that the zero contours (black lines) are straight in all cases, with their slopes depending on the environmental parameters. Furthermore, the leftmost panel of Figure 3 shows that the zero contour of the net sediment transport does not coincide with the zero contour of the migration rate, indicating that the net sediment transport and migration rate do not always point in the same direction. This will be further elaborated on in Section 5.2.

In the sensitivity analysis, we accounted for changes in A_{v} with changing depth H and tidal current amplitude U_{M2}. Furthermore, we have not re-calibrated the slip parameter s on the wavelength of the FGM within the sensitivity analysis, but instead show the wavelength of the FGM in each panel of Figure 3. The qualitative picture of the mechanism remains the same across a wide range of FGM-wavelengths and parameter settings.

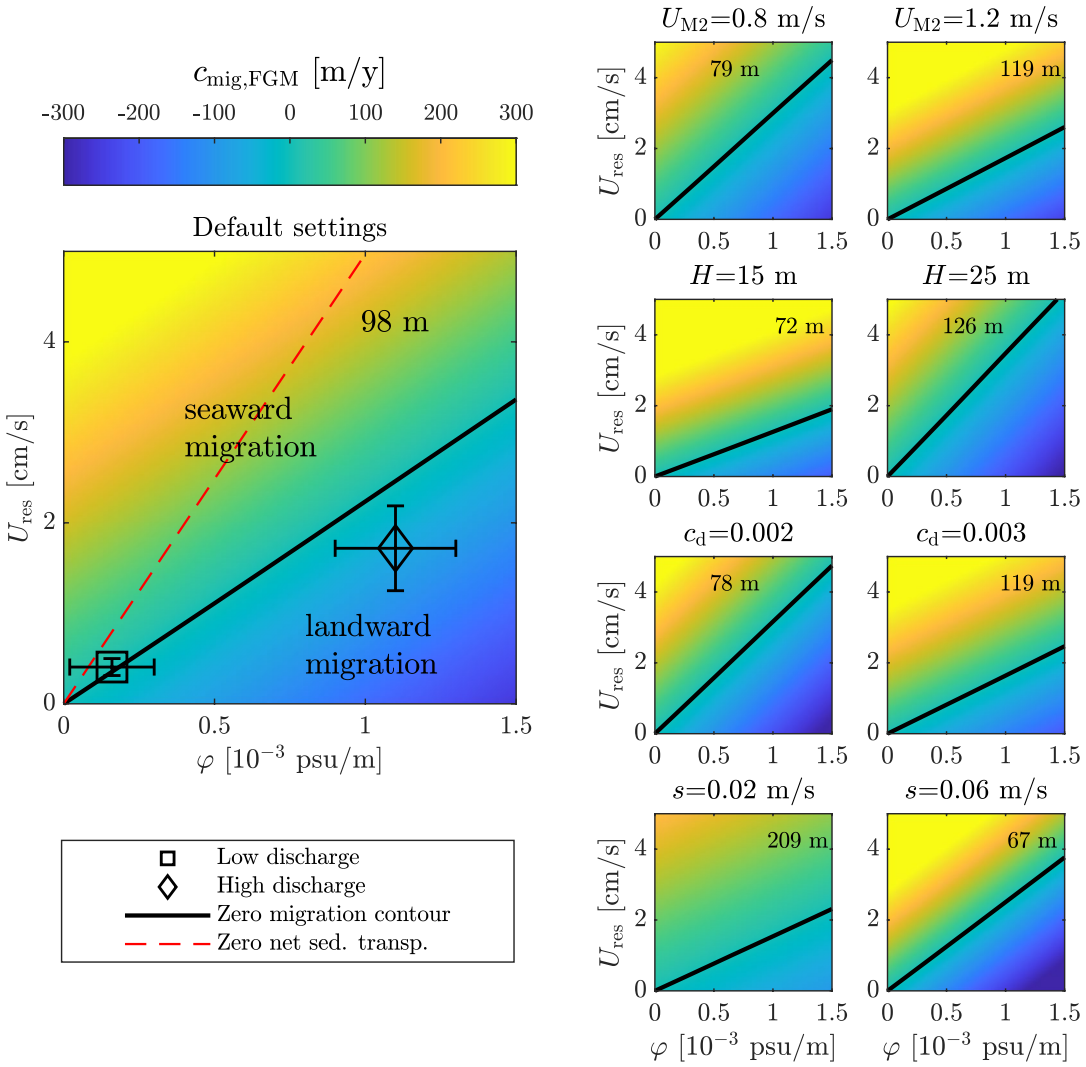

Figure 3. Dependence of the migration rate of the fastest growing mode on the longitudinal salinity gradient and the depth-averaged river flow velocity, for a variety of parameter settings; the corresponding wavelength of the fastest growing mode is given in each panel. The solid black lines represent the zero migration contour, and the red dashed line shows the zero contour of the basic state bed-load transport (further discussed in Section 5.2). The marker symbols with error margins show combinations between U_{res} and φ for low and high discharge in the Gironde estuary.

5. Discussion

Our idealized modeling approach schematizes various processes (e.g., constant eddy viscosity) and isolates two potential drivers of dune migration (i.e., river flow and gravitational circulation). The model results should be interpreted mostly qualitatively: They show a new mechanism of dune migration in estuaries which is of a significant order of magnitude, but precise migration rates cannot be inferred from our model.

5.1. Application to the Gironde

The Gironde setting is reflected in the choice of parameter values (Table 1), which also include a range of forcing conditions during low and high discharge. The longitudinal salinity gradient φ is estimated through visual inspection of the salinity field as obtained by the numerical simulations of van Maanen and Sottolichio (2018). Their figures show that the salinity front is pushed seaward during high discharge, greatly increasing the longitudinal salinity gradient at the sand dune field investigated by Berné et al. (1993) which lies near the mouth of the estuary.

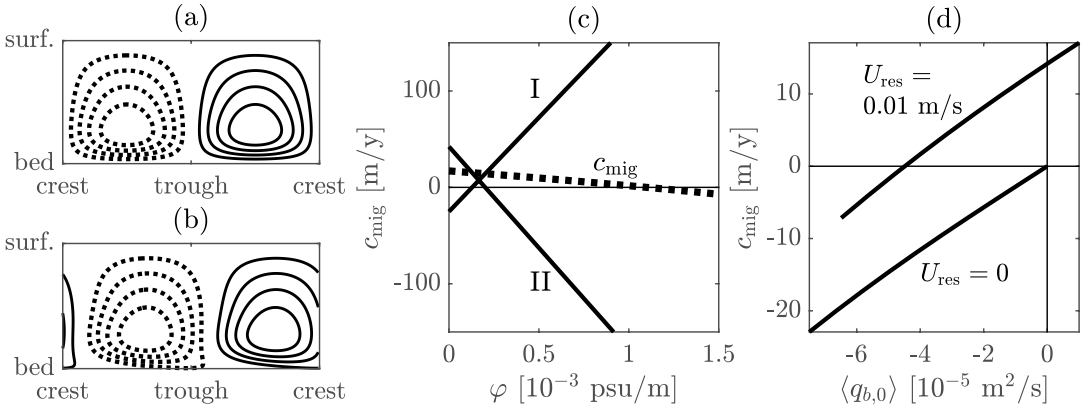

Figure 4. (a, b) Contours of stream functions of the tide-averaged perturbed velocity with dashed line indicating clockwise motion and the solid line counterclockwise. (a) Tide-only and (b) tide with salinity gradient $\varphi = 1 \times 10^{-3}$ psu m^{-1}. (c) Contributions to the migration rate c_{mig} of term I and II which correspond to the underbraced terms in Equation 10; parameters as in Table 1, except $\beta_b = 1$ and $U_{res} = 0.01$ m s^{-1}. (d) Migration rate as a function of the basic state sediment transport; parameter values same as (c).

Residual flow velocities are estimated from $U_{res} = Q_{res}/A$ with discharge values Q_{res} from Berné et al. (1993) and van Maanen and Sottolichio (2018) and cross sectional area $A = 8 \times 10^4$ m^2 estimated from bathymetric charts.

The results, given in Figure 3 (leftmost panel), show that indeed a seasonal reversal of sand dune migration can be explained by the increase of the longitudinal salinity gradient which induces the gravitational circulation. The two cases of the Gironde estuary fall at either side of the $c_{mig,FGM} = 0$-contour, although the error bars for low discharge show that a small salinity gradient may still induce landward migration. Simulations not reported here show that migration rates induced by tidal asymmetry (an alternative driver of dune migration, see Besio et al., 2004) can be of a similar order of magnitude. However, sand dune migration due to tidal asymmetry at the mouth of the Gironde estuary is weak because the phases of the M2 and M4 tidal currents are such that there is no ebb or flood dominance (van Maanen & Sottolichio, 2018).

Overall, our model supports the hypothesis that gravitational circulation caused seasonal reversal of dune migration in the Gironde in the data of Berné et al. (1993), although the idealized nature of the model precludes precise quantitative conclusions.

5.2. Direction of Sediment Transport Versus Direction of Dune Migration

In this section, we aim to unravel the relation between the direction of dune migration and the forcing conditions. Specifically, we will analyze why the red dashed line and the black line in the left panel of Figure 3 do not coincide. To investigate this, we examine the analytical expression for the migration rate:

$$c_{mig} = \frac{\alpha_b \beta_b \left\langle \left|\tau_{b,0}\right|^{\beta_b - 1} \mathrm{Re}(\hat{\tau}_{b,1}) \right\rangle}{(1-p)\hat{h}_{init}}, \qquad \hat{\tau}_{b,1} = \rho s \left[\underbrace{\hat{u}_1}_{\mathrm{I}} + \underbrace{\hat{h}_{init} \frac{\partial u_0}{\partial z}}_{\mathrm{II}} \right] \quad \text{at } z = -H. \tag{10}$$

Here, we have used that $\tau_b = \rho s u$ (Equation 4), and approximated the boundary condition at $z = -H$ through a Taylor expansion (which is one of the steps in the linear stability analysis). Furthermore, $u_1 = \hat{u}_1 \exp(\mathrm{i}kx) + \text{c.c.}$ and $\tau_{b,1} = \hat{\tau}_{b,1} \exp(\mathrm{i}kx) + \text{c.c.}$ For the simplified case with $\beta_b = 1$, the direction of migration is solely dependent on the sign of $\mathrm{Re}(\langle \hat{\tau}_{b,1} \rangle)$, and thus on terms I and II in Equation 10. In further analysis, we will focus on this simplified case.

Term I follows from the solution of the perturbed flow, which can be visualized through a stream function Ψ_1, satisfying $w_1 = \partial \Psi_1 / \partial x$ and $u_1 = -\partial \Psi_1 / \partial z$ (Figures 4a and 4b). The mechanism that explains tidal sand wave formation is a tidally averaged perturbed flow which promotes sediment transport from trough to crest

(Hulscher, 1996). When imposing a longitudinal salinity gradient, these circulation cells are displaced and deformed (Figure 4b).

Figure 4c then shows that term II from Equation 10 decreases with increasing φ as does c_{mig}, whereas term I—the perturbed flow at the bed—acts as a correction on term II. Moreover, Figure 4d shows that the sign of the net sediment transport, given by $\langle q_{b,0} \rangle = \alpha_b \langle | \tau_{b,0} |^{\beta_b - 1} \tau_{b,0} \rangle$ (which equals the sign of term II), does not always equal the sign of the migration rate in the case where there is both a residual current and a longitudinal salinity gradient. This is not the case when $U_{\mathrm{res}} = 0$ (Figure 4d) or when $\varphi = 0$ (not shown here). Hence, for the case of combined barotropic (river) and baroclinic (salinity) forcing, the direction of sand dune migration cannot be directly inferred from the basic flow parameters when the bed shear stress induced by gravitational circulation and river flow are of similar order of magnitude.

6. Conclusion

From a process-based modeling approach using stability analysis, we have shown that gravitational circulation is capable of reversing the migration direction, provided that the river flow velocity is sufficiently small compared to the gravitational circulation. This qualitative picture persists for a variety of parameter settings. Furthermore, the eddy viscosity should be sufficiently small, and the depth relatively large so that the gravitational circulation is strong enough. Hence, the effect of this process on sand dunes can probably also be observed in estuaries that, just like the Gironde, are characterized by a significant salinity gradient and a small residual flow velocity. Lastly, we have shown that the direction of bedform migration is not necessarily the same as the direction of net sediment transport in the basic state.

Appendix A: Expressions for Basic Flow

Expressions of the basic flow are given as follows:

$$u_{0,\mathrm{btr}}^{\mathrm{osc}} = \mathrm{i}\frac{B_{\mathrm{M2}}}{\omega}\left[1 - \frac{\cosh \mu z}{\cosh \mu H + \frac{\mu A_{\mathrm{v}}}{s}\sinh \mu H}\right]\exp(\mathrm{i}\omega t) + \mathrm{c.c.}, \tag{A1}$$

with $\mu = (1 + \mathrm{i})\sqrt{\frac{\omega}{2A_{\mathrm{v}}}}$, and

$$u_{0,\mathrm{bcl}} = -\frac{g\beta H^3 \varphi}{6A_{\mathrm{v}}}\left[\left(\frac{z}{H}\right)^3 + 1 + \frac{3A_{\mathrm{v}}}{Hs}\right], \tag{A2}$$

$$u_{0,\mathrm{btr}}^{\mathrm{steady}} = \frac{B_{\mathrm{res}} H^2}{2A_{\mathrm{v}}}\left[\left(\frac{z}{H}\right)^2 - 1 - \frac{2A_{\mathrm{v}}}{Hs}\right]. \tag{A3}$$

B_{res} and B_{M2} are chosen such that the depth-averaged residual flow velocity equals U_{res}, and the depth-averaged tidal flow amplitude equals U_{M2}. The analytical expression for B_{res} is given by:

$$B_{\mathrm{res}} = -\frac{3}{\tilde{s} + 3}\left[\frac{sU_{\mathrm{res}}}{H} + \frac{1}{8}\varphi g\beta H(\tilde{s} + 4)\right], \qquad \tilde{s} = \frac{Hs}{A_{\mathrm{v}}}. \tag{A4}$$

Data Availability Statement

The source code of the model and scripts to generate the figures of this study are available online at https://zenodo.org/record/4964649; http://10.5281/zenodo.4964649.

Acknowledgments
This work is part of the Perspectief Program Saltisolutions, which is financed by NWO Domain Applied and Engineering Sciences in collaboration with private and public partners. We thank Barend van Maanen for helpful discussions on the Gironde estuary, and we thank two anonymous reviewers for their constructive comments.

References

Allen, J. R. L. (1976). Time-lag of dunes in unsteady flows: An analysis of Nasner's data from the R. Weser, Germany. *Sedimentary Geology*, *15*, 309–321. https://doi.org/10.1016/0037-0738(76)90037-3

Bagnold, R. A. (1956). The flow of cohesionless grains in fluids. *Philosophical Transactions of the Royal Society of London. Series A, Mathematical and Physical Sciences*, *249*, 235–297. https://doi.org/10.1098/rsta.1956.0020

Berné, S., Castaing, P., le Drezen, E., & Lericolais, G. (1993). Morphology, internal structure, and reversal of asymmetry of large subtidal dunes in the entrance to Gironde Estuary (France). *Journal of Sedimentary Petrology*, *63*(5), 780–793. https://doi.org/10.1306/d4267c03-2b26-11d7-8648000102c1865d

Besio, G., Blondeaux, P., Brocchini, M., & Vittori, G. (2004). On the modeling of sand wave migration. *Journal of Geophysical Research*, *109*, C04018. https://doi.org/10.1029/2002JC001622

Best, J. (2005). The fluid dynamics of river dunes: A review and some future research directions. *Journal of Geophysical Research*, *110*(4). https://doi.org/10.1029/2004JF000218

Borsje, B. W., Roos, P. C., Kranenburg, W. M., & Hulscher, S. J. (2013). Modeling tidal sand wave formation in a numerical shallow water model: The role of turbulence formulation. *Continental Shelf Research*, *60*, 17–27. https://doi.org/10.1016/j.csr.2013.04.023

Campmans, G. H. P., Roos, P. C., de Vriend, H. J., & Hulscher, S. J. M. H. (2017). Modeling the influence of storms on sand wave formation: A linear stability approach. *Continental Shelf Research*, *137*, 103–116. https://doi.org/10.1016/j.csr.2017.02.002

Damveld, J. H., van der Reijden, K. J., Cheng, C., Koop, L., Haaksma, L. R., Walsh, C. A., & Hulscher, S. J. M. H. (2018). Video transects reveal that tidal sand waves affect the spatial distribution of benthic organisms and sand ripples. *Geophysical Research Letters*, *45*(21), 11837–11846. https://doi.org/10.1029/2018GL079858

Engelund, F. (1970). Instability of erodible beds. *Journal of Fluid Mechanics*, *42*(2), 225–244. https://doi.org/10.1017/S0022112070001210

Gensen, M. R. A., Warmink, J. J., Huthoff, F., & Hulscher, S. J. M. H. (2020). Feedback mechanism in bifurcating river systems: The effect on water-level sensitivity. *Water*, *12*(7), 1915. https://doi.org/10.3390/w12071915

Geyer, W. R., & MacCready, P. (2014). The estuarine circulation. *Annual Review of Fluid Mechanics*, *46*, 175–197. https://doi.org/10.1146/annurev-fluid-010313-141302

Hansen, D. V., & Rattray, M. (1965). Gravitational circulation in straits and estuaries. *Journal of Marine Research*, *23*(2), 104–122.

Hulscher, S. J. M. H. (1996). Tidal-induced large-scale regular bed form patterns in a three-dimensional shallow water model. *Journal of Geophysical Research*, *101*(C9), 727–744. https://doi.org/10.1029/96JC01662

Knaapen, M. A. F. (2005). Sandwave migration predictor based on shape information. *Journal of Geophysical Research*, *110*(4). https://doi.org/10.1029/2004JF000195

Kostaschuk, R. A., & Best, J. (2005). Response of sand dunes to variations in tidal flow: Fraser estuary, Canada. *Journal of Geophysical Research*, *110*(4). https://doi.org/10.1029/2004JF000176

Meyer-Peter, E., & Müller, R. (1948). Formulas for bed-load transport. In *IAHSR 2nd meeting, Stockholm, appendix 2*. IAHR. (pp. 39–64).

Paarlberg, A. J., Dohmen-Janssen, C. M., Hulscher, S. J., & Termes, P. (2009). Modeling river dune evolution using a parameterization of flow separation. *Journal of Geophysical Research*, *114*(F1). https://doi.org/10.1029/2007JF000910

Prandle, D. (1985). On salinity regimes and the vertical structure of residual flows in narrow tidal estuaries. *Estuarine, Coastal and Shelf Science*, *20*, 615–635. https://doi.org/10.1016/0272-7714(85)90111-8

van der Sande, W. M., Roos, P. C., Gerkema, T., & Hulscher, S. J. M. H. (2021). *Matlab code for "Gravitational circulation as driver of upstream migration of estuarine sand dunes"*. Zenodo. https://doi.org/10.5281/zenodo.4964649

van Haren, J. J. M., & Maas, L. R. M. (1987). Observations on the vertical structure of tidal and inertial currents in the central North Sea. *Journal of Marine Research*, *45*(2), 293–318. https://doi.org/10.1357/002224087788401106

van Maanen, B., & Sottolichio, A. (2018). Hydro- and sediment dynamics in the Gironde estuary (France): Sensitivity to seasonal variations in river inflow and sea level rise. *Continental Shelf Research*, *165*, 37–50. https://doi.org/10.1016/j.csr.2018.06.001

van Santen, R. B., de Swart, H. E., & van Dijk, T. A. (2011). Sensitivity of tidal sand wavelength to environmental parameters: A combined data analysis and modelling approach. *Continental Shelf Research*, *31*(9), 966–978. https://doi.org/10.1016/j.csr.2011.03.003